Macromolecules

Article

pubs.acs.org/Macromolecules

The PCPDTBT Family: Correlations between Chemical Structure, Polymorphism, and Device Performance

G. L. Schulz,[†] F. S. U. Fischer,[†] D. Trefz,[†] A. Melnyk,[‡,§] A. Hamidi-Sakr,[∥] M. Brinkmann,[∥] D. Andrienko,[‡] and S. Ludwigs*[,†]

[†]IPOC-Functional Polymers, University of Stuttgart, Pfaffenwaldring 55, 70569 Stuttgart, Germany

[‡]Max Planck Institute for Polymer Research, Ackermannweg 10, 55128 Mainz, Germany

[§]Graduate School Materials Science in Mainz, Staudinger Weg 9, 55128 Mainz, Germany

[∥]Institut Charles Sadron, CNRS, University of Strasbourg, 23 rue du loess, 67034 Strasbourg, France

Supporting Information

ABSTRACT: We highlight the influence of processing conditions on polymorphism and structure formation on the mesoscale for the family of PCPDTBT polymers with branched alkyl side chains. Direct correlations of morphology to the chemical structure and to transistor device performance are established. We found that up to four different packing motifs could be realized depending on the polymer derivative and the processing conditions: amorphous, π-stacked, cross-hatched and dimer-containing polymorphs. While C- and F-PCPDTBT display similar packing behavior organizing in π-stacked and dimer-like structures, Si-PCPDTBT gives rise to cross-hatched structures upon simple deposition from solution. The observed differences in chain packing for C-/F-PCPDTBT versus Si-PCPDTBT are attributed to differences in backbone conformations and aggregation behavior in solution. The effect of polymorphism on charge transport is probed using field-effect transistors, in which both π-stacked and cross-hatched polymer chain arrangements yield the highest hole mobilities. Mesoscopic morphology and mobility simulations rationalize our experimental findings by relating mobility to distributions of electronic coupling elements between the chains.

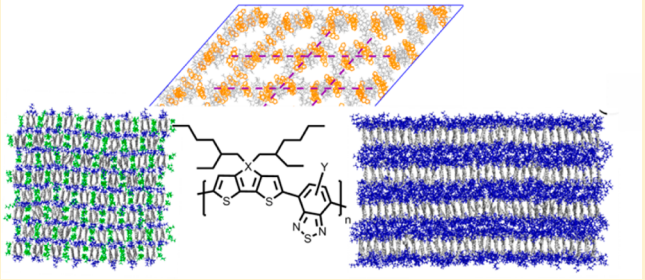

1. INTRODUCTION

The study of the morphology of conjugated polymers has been an active area of research for several decades due to its well-established role in influencing their many optoelectronic properties such as light absorption and charge transport. Regioregular poly(3-hexylthiophene) (P3HT), for example, is a semicrystalline polymer which has been shown to demonstrate various packing motifs, depending on the deposition conditions, from amorphous to highly ordered $\pi-\pi$ stacked arrangements. P3HT polymer chains crystallize in various orientations with respect to the substrate, from face-on to edge-on to standing chains.[1] Pioneering work in this field was done by Sirringhaus and co-workers,[2] who investigated the effect of different P3HT chain orientations on the transistor properties. In edge-on orientation, the field effect mobility is more than 100 times higher than for chains in face-on orientation, which is explained by excellent charge transport along the chain axis and in the π-stacking direction.[3,4] In our studies we found that for example solvent vapor annealing could be used to precisely control the crystallization of P3HT.[5] Charge transport in anisotropic thin films was preferred along the polymer chains over transport in the $\pi-\pi$ stacking direction.[6] Another conjugated polymer that has also been given much attention is poly(9,9-dioctylfluorene) (PFO).[7] PFO has two reported polymer conformations: α and β. The β-type conformation prevails in PFO thin films exposed to vapors of good solvents, e.g., toluene, whereas the α chain conformation is reported to crystallize in a dimer-containing orthorhombic structure of high symmetry (*Pnb*21) and to have a less planar backbone than the β conformation.[8,9]

Over the years a new class of conjugated polymers, namely donor−acceptor (D−A) copolymers, has been developed. In comparison to P3HT and PFO, fewer studies have been performed on the precise packing motifs of these, more advanced, materials.

D−A copolymers are structurally more complex than homopolymers like P3HT and PFO, since they consist of electron-rich and electron-poor π-conjugated building blocks. A typical example of a D−A copolymer is poly[*N*,*N*′-bis(2-octyldodecyl)-1,4,5,8-naphthalenedicarboximide-2,6-diyl]-*alt*-5,5′-(2,2′-bithiophene) (P(NDI2OD-T2)). This low band gap copolymer has demonstrated impressive optoelectronic properties and has found application in organic field-effect transistors (OFETs)[10] and organic solar cells[11] as an n-type semi-

Received: August 5, 2016
Revised: January 23, 2017
Published: February 9, 2017

DOI: 10.1021/acs.macromol.6b01698
Macromolecules 2017, 50, 1402−1414

conductor. Because of the alternating nature of the chemical structure, new packing motifs in comparison to homopolymers such as segregated and mixed stacking of the donor and acceptor blocks are possible. Two polymorphs of the semicrystalline P(NDI2OD-T2) (known as form I and form II) have been induced in thin films by applying different temperature annealing protocols.[12,13] Another example of a D−A polymer is the p-type semiconductor poly[2,6-(4,4-bis(2-ethylhexyl)-4*H*-cyclopenta[2,1-*b*;3,4-*b*′]dithiophene)-*alt*-4,7-(2,1,3-benzothiadiazole)] (C-PCPDTBT), which consists of alternating cyclopentadithiophene (CPDT, donor) and benzothiadiazole (BT, acceptor) units (for chemical structure see Scheme 1). C-PCPDTBT was introduced in 2006 by Brabec and co-workers, in an attempt to reduce the band gap and thus to increase efficiency of a bulk heterojunction solar cell. Indeed, promising power conversion efficiencies (PCEs) up to 3.16% were demonstrated.[14] In the following year, Peet and Bazan reported that solvent additives instead of thermal annealing can lead to PCEs up to 5.5% for C-PCPDTBT:$PC_{71}BM$ blends.[15] Further studies indicated that the presence of solvent additive 1,8-diiodooctane (DIO) could improve blend morphology and interchain coupling as a result of enhanced $\pi-\pi$ stacking.[16,17] Later, an edge-on orientation of the C-PCPDTBT polymer chains could be identified using grazing incident X-ray diffraction techniques (GIXRD) by Nelson,[17] Bazan,[18,19] and Russell and co-workers.[20]

Scheme 1. Chemical Structure and Molecular Weight of the Three PCPDTBT-Based Polymers Described in This Study

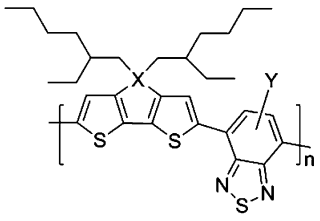

C-PCPDTBT: X = C, Y = H
Si-PCPDTBT: X = Si, Y = H
F-PCPDTBT: X = C, Y = F

	C-PCPDTBT	F-PCPDTBT	Si-PCPDTBT
M_w (kg/mol)	26.7	10.8	32.3
M_n (kg/mol)	14.7	6.7	11.0
PDI	1.8	1.6	2.9

Considering the promising nature of C-PCPDTBT, structural modifications on the polymer backbone have also been investigated over the past decade. In 2012, Neher[21] and Jen[22] both reported on a fluorinated PCPDTBT derivative by replacing one of the hydrogen atoms on the benzothiadiazole ring with a fluorine atom, yielding a regiorandom copolymer: poly[2,6-(4,4-bis(2-ethylhexyl)-4*H*-cyclopenta[2,1-*b*;3,4-*b*′]-dithiophene)-*alt*-4,7-(5-fluoro-2,1,3-benzothiadiazole)] (F-PCPDTBT). PCEs up to 6.6%[23] were reported for F-PCPDTBT:$PC_{71}BM$ blends as well as hole mobilities of 10^{-2} $cm^2/(V\ s)$ in organic field-effect transistors (OFETs).[24] Several years earlier, in 2008, Yang had described another low band gap polymer in which the bridging carbon atom in the cyclopentadithiophene building block was replaced with a silicon atom: poly[(4,4′-bis(2-ethylhexyl)dithiene-[3,2-*b*:2′,3′-*d*]silole)-*alt*-4,7-(2,1,3-benzothiadiazole)] (Si-PCPDTBT).[25] For the Si containing derivative, PCEs of 5.1% were obtained as well as hole mobilities up to 10^{-2} $cm^2/(V\ s)$ were measured in OFETs.[26] Further investigations of Si-PCPDTBT were carried out by Neher and co-workers, who implemented multiple fullerene derivatives with Si-PCPDTBT to study the charge transfer state splitting in solar cells.[27]

The differences in charge transport and photovoltaic properties of these three structurally similar low band gap polymers are often rationalized by the strength of their $\pi-\pi$ stacking interactions. The arguments used to support these claims are analogous to those applied to the P3HT semicrystalline morphology. For Si- and C-PCPDTBT, an edge-on morphology has been proposed, and the relative crystallinities of the two were compared using GIXRD techniques. The silicon-containing derivative is more crystalline than C-PCPDTBT and has displayed $\pi-\pi$ stacking distances as low as 3.48 Å versus 3.6−3.8 Å for C-PCPDTBT.[20,28,29] Such close packing of the polymer backbone is attributed to the longer Si−C bond versus the C−C bond connecting the solubilizing branched alkyl chains to the aromatic units for Si- and C-PCPDTBT, respectively. In the case of F-PCPDTBT versus C-PCPDTBT, the stronger $\pi-\pi$ interactions of the fluorinated derivative were attributed to intra or intermolecular F−F or H−F interactions.[21,22,24]

As a part of our own investigations on the family of PCPDTBT polymers, we have examined the behavior of C-PCPDTBT in solution[30] and the thin film morphology[31,32] as well as compared the structure and polymorphism of C- versus F-PCPDTBT.[33] In this report we complete the series with inclusion of the silicon-bridged analogue of PCPDTBT which shows yet another polymorph.

In what follows, we describe the processing techniques used to obtain various polymorphs as well as their characteristic traits, starting with C-PCPDTBT, followed by F-PCPDTBT and finally Si-PCPDTBT. This includes structural characterization and measurements of charge carrier mobilities of all polymers in different polymorphs under identical conditions. The experimental results are supported by theoretical calculations performed for the predicted crystalline packing motifs. To this end, we use molecular dynamics simulations to simulate atomistic morphologies of large supercells and evaluate charge transfer rates using polarizable force fields and first-principles methods. Kinetic Monte Carlo (KMC) simulations are then used to solve the master equation for charge dynamics. Finally, we evaluate charge mobility from the KMC trajectories. Simulation results on structures and mobilities are compared to experimental data allowing us to rationalize the molecular packing and the effect of local and mesoscale ordering on charge carrier mobility.

2. RESULTS AND DISCUSSION

2.1. Chemical and Physical Properties. Scheme 1 shows the chemical structures and molecular weights of three PCPDTBT-based polymers. The molecular weight measurements were performed using high temperature size exclusion chromatography against polystyrene standards. All three polymers have low molecular weights: number-average molecular weights (M_n) amount to 14.7, 6.7, and 11.0 kg/mol for C-PCPDTBT, F-PCPDTBT, and Si-PCPDTBT, respectively.

2.2. Morphology and Charge Transport Simulations. We start by rationalizing the differences in hole mobilities

DOI: 10.1021/acs.macromol.6b01698
Macromolecules 2017, 50, 1402−1414

exhibited by the three PCPDTBT derivatives: Si- and F-PCPDTBT can have hole mobilities up to 10^{-2} $cm^2/(V\ s)$, whereas the mobility of C-PCPDTBT is approximately 1 order of magnitude lower at 10^{-3} $cm^2/(V\ s)$ (see Table S1).[22,25,26,28,29,34,35] These charge transport measurements were obtained from classical deposition conditions reported to yield mainly π-stacked structures. At this stage it remains unclear whether the change in the electronic structure, local molecular packing, or mesoscale ordering of chains in the film is responsible for the change in the hole mobility.

To rule out contributions due to the change in the electronic structure, we first analyze electronic coupling elements (transfer integrals) between two tetramers (four donor−acceptor pairs) in a π-stacked arrangement. These couplings are plotted as a function of the relative shift d between two backbones in Figure 1. The separation between two chains is fixed to 4.0 Å; d = 0 Å

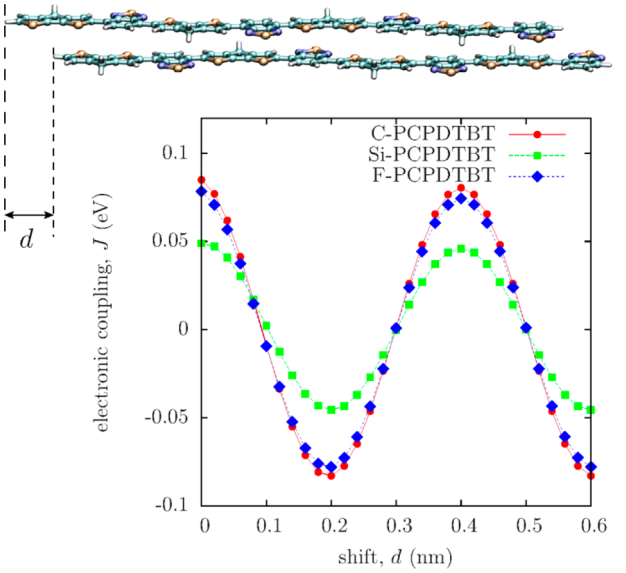

Figure 1. Electronic coupling element between two backbones (tetramers with side chains substituted by hydrogens) versus the backbone−backbone shift d. Backbones are parallel to each other and constrained to a fixed separation of 4 Å. Electronic couplings are evaluated using the projection method,[36] B3LYP density functional, and 6-31g basis set.[37] The monomer length of 11.8 Å is similar for all three derivatives.

corresponds to a geometry of a dimer in a π-stack morphology with a minimal side-chain overlap, i.e., when the acceptor (BT) units are on top of each other, while the donor (CPDT) units are spatially separated due to backbone bending, as shown in Figure 7a,b. In this model system, branched ethylhexyl side chains are replaced with hydrogens in order to reduce computational costs.

Evidently, all three polymers have a similar dependence of the electronic coupling on the relative shift d. Si-PCPDTBT has the lowest coupling for this given dimer geometry (see Supporting Information, Sections B and C, for details). This observation is in a clear contradiction to the experimental observations, with Si-PCPDTBT having the highest OFET mobilities. We can therefore conclude that the change in the electronic structure alone cannot be responsible for the change in charge mobility. Hence, different polymers have different mesoscale ordering of backbones.

To further assess the influence of chain packing on charge transport, we have performed molecular dynamics simulations of large supercells of 128 π-stacked tetramers with ethylhexyl side chains. The simulation box of 4 lamellae with 32 chains per lamella has been equilibrated at 300 K and ambient pressure using Berendsen thermostat and barostat.[38] Typical simulated morphologies are shown in Figures 3a (unit cell) and 3b (supercell). The corresponding unit cell parameters are similar for C- and F-PCPDTBT: π-stacking distance is 3.8 Å, and interlamellar spacing is 16.7 Å. In the case of Si-PCPDTBT the corresponding values are 3.7 and 17.6 Å. We then used 10 snapshots of the 1 ns production run in order to perform averages of the distribution of electronic coupling elements, site energies, and mobilities.

Electronic coupling elements were evaluated using the projection method[36] with diabatic states constructed from HOMO energy levels of hydrogen-saturated tetramers. With the electronic couplings at hand, we have evaluated intermolecular charge transfer rates using the high-temperature limit of nonadiabatic charge transfer theory:[39]

$$k_{A\to B} = \frac{2\pi}{\hbar}\frac{J_{AB}^{\ 2}}{\sqrt{4\pi\lambda k_B T}}\exp\left[-\frac{(\Delta U_{AB}-\lambda)^2}{4\lambda k_B T}\right]$$

Here $\lambda \approx 0.1$ eV is the reorganization energy, J_{AB} the electronic coupling, and $\Delta U_{AB} = U_A - U_B$ the driving force. All these parameters were evaluated using a combination of quantum-chemical methods and classical polarizable force fields.[40,41]

The rates and centers of mass of molecules were used to parametrize the master equation which was solved using the kinetic Monte Carlo (KMC) algorithm.[42] The intermolecular charge-carrier mobility along the direction of the external field $\vec{E}$ was obtained from the charge trajectory as

$$\mu = \frac{\langle \Delta\vec{R}\cdot\vec{E}\rangle}{\Delta t|\vec{E}|^2}$$

where $\Delta\vec{R}$ is the displacement of charge over a simulation time Δt. The electric field of 10^6 V/m is applied along the π-stacking axis. The results of simulations are summarized in Table 1.

Table 1. Summary of Transistor Characteristics of the π-Stacked Polymers[a]

π-stacked structures	μ_{sim} $(cm^2/(V\ s))$
C-PCPDTBT	7.8×10^{-2}
F-PCPDTBT	10.5×10^{-2}
Si-PCPDTBT	18.6×10^{-2}

[a]Simulated mobility (μ_{sim}) values are given without taking into account energetic disorder (i.e., assuming high charge carrier densities in OFETs). Averaging is based on 1280 points for each system; the largest error is less than 10^{-3} $cm^2/(V\ s)$. With energetic disorder, the simulated mobility is less than 10^{-6} $cm^2/(V\ s)$.

Since we do not take into account energetic disorder and defects, such as grain boundaries and amorphous regions, the calculated mobilities are higher than the experimental ones. The trend is, however, clear: the carbon-bridged polymer has the lowest and the silicon-based PCPDTBT the highest mobility. Hence, we can conclude that the local chain packing favors larger hole mobility in Si-PCPDTBT. This can indeed be confirmed by looking at the distributions of electronic couplings in the simulated morphologies (see Supporting Information, Section A and Figure S4): Si-PCPDTBT has the

DOI: 10.1021/acs.macromol.6b01698
Macromolecules 2017, 50, 1402−1414

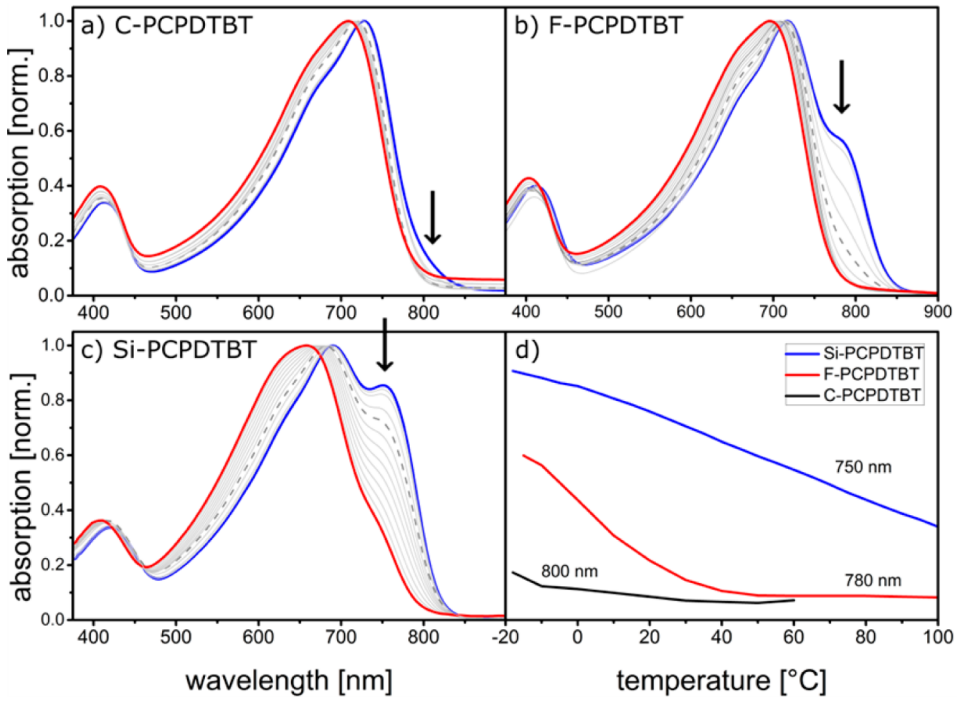

Figure 2. Temperature-dependent absorption spectra of polymer solutions in CB (1 mg/mL): (a) C-PCPDTBT, (b) F-PCPDTBT, and (c) Si-PCPDTBT, measured in the temperature range between 100 °C (red) and −15 °C (blue) with 10 °C temperature steps shown in gray. Spectra measured at RT shown as dashed line. (d) Change in intensity of the shoulder at long wavelengths (750−800 nm) as a function of temperature for the three PCPDTBT polymers.

largest average coupling. Better registry of backbones in Si-PCPDTBT could be attributed to longer Si−C bonds and softer attachment of alkyl side chains due to a larger, as compared to carbon, Si atom.[43] Indeed, the side chains of Si-PCPDTBT are on average further away from the backbone, leading to larger interlamellar separations and, correspondingly, smaller $\pi-\pi$ distances. Energetic disorder in the lamellar arrangements of all three polymers is rather large, in part due to conformational disorder of side chains. If accounted for it leads to at least 3 orders of magnitude decrease of mobility (at low charge carrier densities) for all three polymers.

Even though the local ordering already favors transport in Si-PCPDTBT as compared to other derivatives, the difference in simulated mobilities is still smaller than measured in OFETs. This indicates that large-scale molecular arrangement further favors transport in Si-PCPDTBT.

2.3. Aggregation in Solution. As start of our experimental investigations, we first compare the aggregation behavior of all PCPDTBT derivatives using temperature-dependent UV−vis absorption spectroscopy (Figure 2). Through the appropriate choice of solvent and a wide temperature window, one can in an ideal case observe a transition from the fully dissolved (high temperature) to the highly aggregated state (low temperature). Before going into detail about the absorption spectra of each polymer, it should also be noted that for all PCPDTBT polymers the high-energy band seen at around 400 nm and the low-energy band at about 700 nm are assigned to a $\pi-\pi^*$ and charge transfer transition, respectively.[30] Figure 2a displays the measured absorption profiles for C-PCPDTBT in CB from −15 (blue) to 100 °C (red). From high temperature down to room temperature, the maximum absorption wavelength was found to be at 710 nm, and the spectral shape can be described as rather broad with a slight shoulder at high energy (~660 nm). Cooling toward −15 °C (spectrum shown in blue), a 15 nm red-shift of the absorption maximum up to 725 nm is observed. In a recent publication we have described the aggregation behavior of C-PCPDTBT in 2-methyltetrahydrofuran (m-THF) between −93 and 67 °C using absorption and photoluminescence spectroscopy. These experiments in combination with an evaluation via Franck−Condon analysis revealed an isosbestic point and thus two polymer conformations: a disordered random coil and an aggregated conformer with planarized chains.[30] At low temperatures, the aggregated phase of C-PCPDTBT consisted of long-range $\pi-\pi$ stacked polymer chains (a clear absorption peak at 800 nm is indicative). Both in m-THF and in THF, PCPDTBT is slightly more aggregated at room temperature (compare Figure S1).

For the F-PCPDTBT polymer, the temperature-dependent absorption spectra are displayed in Figure 2b. The spectrum measured at 100 °C shows a maximum absorption at 690 nm, with a hint of a shoulder at 660 nm. At room temperature, the maximum is shifted to 710 nm. Upon further cooling to −15 °C, λ_{max} is at 720 nm and a shoulder at 780 nm becomes clearly visible.

Si-PCPDTBT displays analogous trends in its absorption behavior as the other two polymers, but with much stronger aggregation tendency. At 100 °C (Figure 2c, red spectrum), the maximum absorption is at 655 nm, whereas at 20 °C and lower temperatures two distinct maxima at 655 and 750 nm become visible.

In Figure 2d, the decay of the aggregated species in solution is depicted by plotting the absorption intensity evolution of the low-energy peak (750−800 nm) as a function of temperature for all three polymers. For C-PCPDTBT, no clear shoulder can be observed, indicating that very little aggregation occurs in chlorobenzene solution (refer to Figure 2a). For F-PCPDTBT, the shoulder at 780 nm is less intense than for Si-PCPDTBT and decreases steadily in intensity from −15 to 40 °C. The

DOI: 10.1021/acs.macromol.6b01698
Macromolecules 2017, 50, 1402−1414

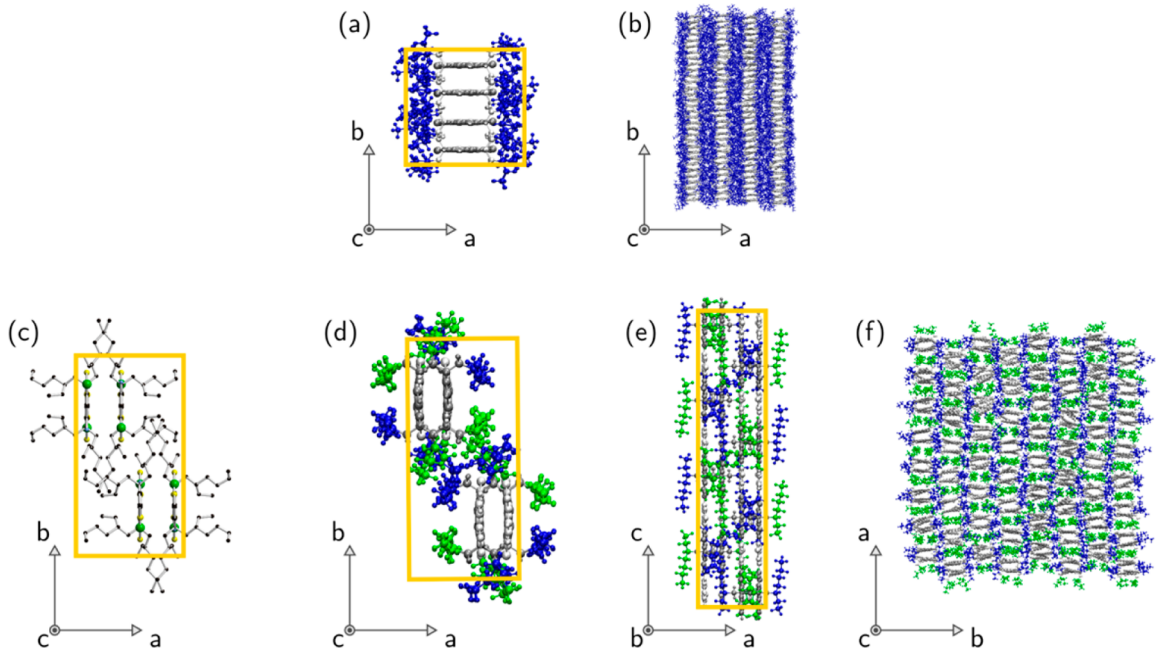

Figure 3. Schematic illustration of the unit cells of the PCPDTBT polymorphs: (a) π-stacked unit cell and (b) supercell, equilibrated using molecular dynamics. Dimer-containing unit cell of F-PCPDTBT: (c) proposed crystal structure from experimental studies,[33] (d–f) after equilibration using molecular dynamics simulations. The final unit cell dimensions are given in Table 2. The π-stacked polymorph has been observed for all C-, Si-, and F-PCPDTBTs, whereas the dimer-like structure only for F-PCPDTBT[33] and C-PCPDTBT.[32,33]

silicon-containing polymer, however, displays a shoulder at 750 nm over the entire temperature range. The results clearly indicate the tendency to undergo aggregation increases in the series C-PCPDTBT, F-PCPDTBT, Si-PCPDTBT. Depending on the solvent in which the polymer is dissolved, the aggregates can be present in solution at room temperature, for example, like the case of Si-PCPDTBT in CB or C-PCPDTBT in THF (refer to Figure S1) but not for C-PCPDTBT in CB (see Figure 2). Additionally, we further observed a significant decrease in polymer solubility from C-PCPDTBT to F-PCPDTBT to Si-PCPDTBT. We note that materials with low solubility can in extreme cases limit the processing and characterization techniques that can be applied to study such conjugated polymer systems. Later during the spin-coating process, aggregation in solution becomes important because it influences structure formation if preaggregated species are deposited from solution or if aggregates form during the drying process.

2.4. C- and F-PCPDTBT. The film morphology of a conjugated polymer is influenced by a variety of factors such as chain rigidity, molecular weight, length and density of alkyl side chains, solubility, aggregation, and crystallinity, etc. It has been found that subtle changes in chemical structure, e.g., the inclusion of a fluorine atom on a benzothiadiazole unit (as is the case for F-PCPDTBT versus C-PCPDTBT) or variations of the solubilizing side chains, can result in significant changes in polymer properties.[21,22,34,44] The protocol and the solvent used to fabricate the thin films play an equally important role in determining the final morphology, as shown for example in depth for P3HT as model system.[1,45] Finally, after film formation, further modification of the morphology can be achieved by thermal or solvent annealing. In the upcoming section it will be shown how chemical structure, deposition technique, and postdeposition treatment influence polymer film morphology for C- and F-PCPDTBT.

To date, the PCPDTBT polymers have been shown to demonstrate up to three different morphologies: amorphous, π-stacked, and the more recently reported "dimer" structure.[32,33] The latter two packing motifs are depicted in Figure 3 as a point of reference for the reader. Figures 3a and 3b depict the polymer chain arrangement of the π-stacked polymorph after equilibration using molecular dynamic simulations. The long-range π-stacked structure of C-PCPDTBT (and its Si analogue) has been proposed based on the results of GIXRD experiments. It is noteworthy to mention that such π-stacked structures are typically attributed to an edge-on orientation.[20,28]

In addition, both F- and C-PCPDTBT form semicrystalline lamellar morphologies whose crystal structure has been assigned to the *Pccn* space group which is very similar to that which has been reported for α-PFO (*Pnb*21).[33] The orthorhombic unit cell contains four polymer chains grouped into pairs (dimers, Figure 3c,d). CPDT and BT units are stacked in a segregated manner in the dimers, forming stacked PCPDTBT polymer chains. The alkyl side chains are surrounding the two planar backbones and insulate the individual dimer units from one another. An important finding that has emerged during the investigations of the dimer crystal structure is that it is thermodynamically more stable than the π-stacked polymorph.[33]

The proposed dimer-like polymer arrangement for C-PCPDTBT and F-PCPDTBT is examined in more detail in refs 32 and 33. Figure 3c exemplarily shows the projection of the crystal structure of F-PCPDTBT in the *ab* plane. It has to be noted that the $\pi-\pi$ stacking distance between two chains within a dimer was estimated to be between 3.6 and 3.8 Å; no long-range π stacking is possible in these structures. In order to validate the experimentally predicted unit cell of a dimer structure, we have additionally performed molecular dynamics simulations with this molecular arrangement. Supercells (4×8 unit cells, with four tetramers in each unit cell) were

DOI: 10.1021/acs.macromol.6b01698
Macromolecules 2017, 50, 1402–1414

constructed from the proposed unit cells and equilibrated at 300 K and ambient pressure for 1 ns. All supercells were stable during the entire equilibration run. As an example, the final unit cell and supercell for F-PCPDTBT are shown in Figure 3d–f. The unit cell dimensions, summarized in Table 2, are in good agreement with experiment. Note that even though our simulations support experimental findings only indirectly (since free energy calculations of large supercells are computationally prohibitive), a combination of molecular dynamics simulations and TEM/ED allows the identification of detailed molecular arrangements in unit cells, accounting for the excluded volume of branched side chains.

Table 2. Comparison of the Unit Cell Parameters for the Orthorhombic Structures of the Dimer-Containing Polymorphs obtained Experimentally (ED) and from Molecular Dynamics Simulations

	c (along the backbone, nm)	*b* (nm)	*a* (nm)
C-PCPDTBT (simulated)	2.46	2.08	1.25
C-PCPDTBT (experiment[33])	2.36	1.93	1.24
F-PCPDTBT (simulated)	2.40	2.20	1.17
F-PCPDTBT (experiment[33])	2.32	2.06	1.10

2.4.1. Preparation Conditions–Structural Analysis. Next we present the preparation techniques which can be used to obtain the various polymer morphologies as well as their characteristic traits. The thin film morphology of C-PCPDTBT spin-coated from two different solvents ($CHCl_3$ and CB/DIO) are shown using atomic force microscopy (AFM) height images in Figures 4a and 4b, respectively. The sample deposited using chloroform displays no characteristic features in the AFM images (Figure 4a), and the corresponding absorption profile is broad and featureless (see Figure 4d).[31] These results as well as the rather fuzzy and weak π-stacking reflection in the ED pattern (Figure S5e) led us to the conclusion that the sample spin-coated from chloroform is rather amorphous in nature. In contrast, films deposited from a high boiling point mixture of CB and DIO yielded excellent solar cell performance,[15] and polymer chains have extended $\pi-\pi$ stacking interactions as suggested from a rather sharp and intense Scherrer ring at 3.75 Å in the ED pattern (see Figure S6). Such π-stacked aggregates have also been observed for P3HT and for P3HT, they consist of an edge-on orientation with respect to the substrate.[20,28] The AFM height image shown below reveals round aggregates on the film surface, approximately 40 nm in diameter (Figure 4b). A distinct shoulder at 800 nm can be seen in the absorption spectrum of the thin film spin-coated from CB/DIO (Figure 4d). In analogy to the peak assignment performed in temperature-dependent absorption spectroscopy experiments,[30] in the thin films spin-coated from CB/DIO we also assign the presence of the shoulder at long wavelength to ordered, π-stacked, C-PCPDTBT polymer chains.

DIO and other high boiling point solvents (e.g., 1-CN) are needed for C-PCPDTBT to force the polymers in the long-range π-stacked structure; preaggregation in solution seems to play a major role in this context (compare section 2.3).

To access the dimer crystal structure, we found that melt crystallization on PTFE films and solvent vapor annealing of spin-coated films can be used[32,33] (compare Figure S7e,h). Using the latter approach with carbon disulfide as solvent vapor homogeneous films are accessible (Figure 4c). Fiber-like

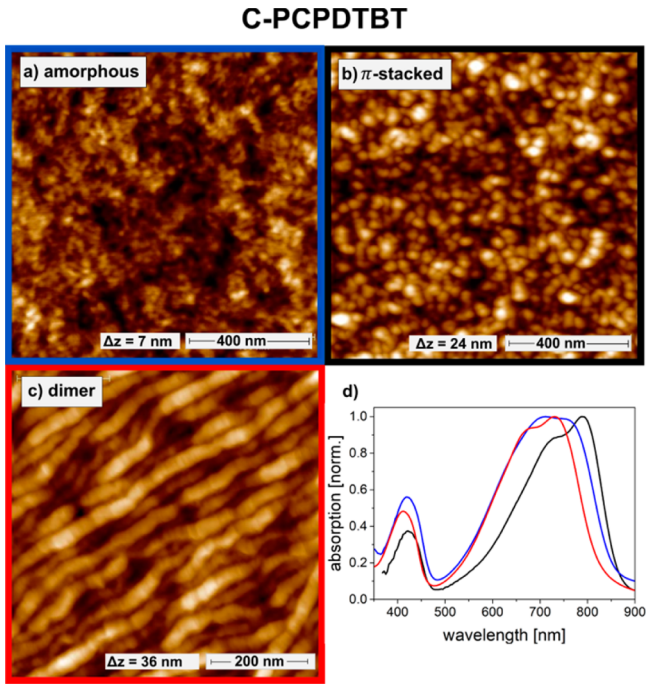

Figure 4. AFM height images (1 × 1 μm) of C-PCPDTBT: (a) spin-coated from $CHCl_3$ yielding a mainly amorphous film, (b) spin-coated from CB/DIO yielding the π-stacked structure, and (c) spin-coated from $CHCl_3$ and exposed to CS_2 vapor afterward, yielding the dimer crystal structure. (d) Absorption spectra of thin films: spin-coated from $CHCl_3$: blue; spin-coated from CB/DIO: black; and after exposure to CS_2 vapor: red. For further morphological data on C-PCPDTBT we refer to Figures S5–S7.

structures with a diameter of 40 nm can be seen on the surface in the AFM height image. The absorption spectra of the solvent annealed film show a blue-shift of the maximum of about 60 nm compared to the film spin-coated from CB/DIO and a pronounced shoulder at 650 nm. Using TEM/ED (Figure S7e,h) and GIWAXS measurements (Figure S7f), the film exposed to solvent vapor was confirmed to adopt the dimer structure (compare simulated structures in Figure 3c–f). Figure S7h shows the characteristic traits in the ED pattern for C-PCPDTBT in the dimer arrangement with 110 and 004 reflections, displayed at 10.5 and 5.9 Å, respectively.[33,46]

To summarize, three different polymer morphologies were obtained for the C-PCPDTBT derivatives: amorphous, π-stacked, and dimer crystal structure. Our data show no evidence for coexistence of the π-stacked and dimer polymorphs.

A similar approach was applied to samples consisting of F-PCPDTBT. Interestingly no amorphous films were accessible by solution deposition. Spin-coating from a solvent with a high boiling point such as chlorobenzene led to rod-like structures (diameter around 30 nm) in the AFM height image shown in Figure 5a. TEM also revealed rod-like structures whereas the ED pattern shows an intense π-stacked ring at 3.7 Å and a weak ring with a 11.0 Å interlayer spacing (see Figure S8). These reflections point indeed at a π-stacked structure with a dominant population of edge-on oriented crystals.

The corresponding absorption profile of the same thin film shows a band centered around 750 nm with an intense shoulder at 790 nm (Figure 5e). The shoulder observed at 790 nm is assigned to aggregates in the thin film that are of the same nature as those seen in the CB solution at −15 °C (Figure 2b) which consist of long-range π-stacked polymer chains. For the

DOI: 10.1021/acs.macromol.6b01698
Macromolecules 2017, 50, 1402–1414

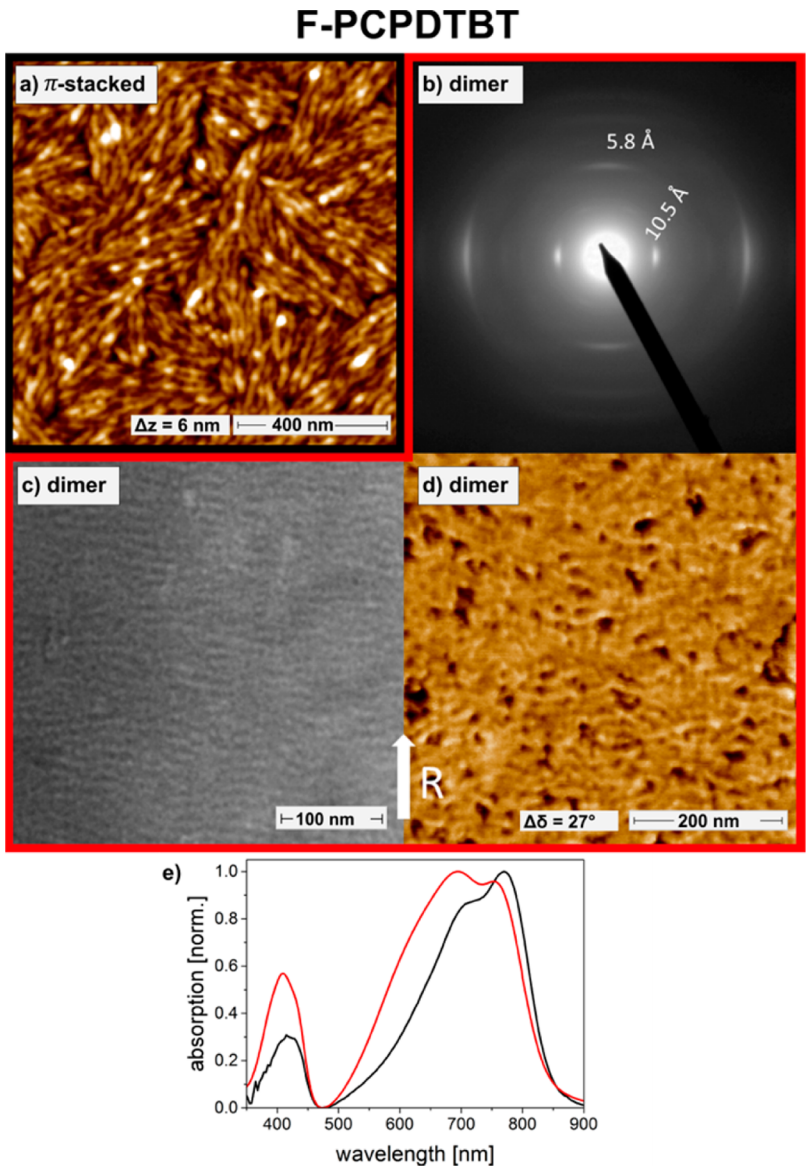

Figure 5. AFM height image of F-PCPDTBT spin-coated from CB (a) exhibiting a π-stacked morphology. ED pattern (b), bright field TEM image (c), and AFM phase image (d) of a thin film of F-PCPDTBT after HT rubbing at 240 °C.[33] White arrow indicates the rubbing direction. (e) Corresponding absorption spectra of the π-stacked and dimer-containing structures, black and red lines, respectively. For further morphological data on F-PCPDTBT we refer to Figures S8 and S9.

carbon-bridged analogue of PCPDTBT, additives with high boiling points such as diiodooctane (bp 365 °C) were needed to induce the $\pi-\pi$ stacking; however, for F-PCPDTBT, chlorobenzene (bp 132 °C) was sufficient since it has a higher tendency to aggregate in solution than C-PCPDTBT.

Again solvent vapor annealing had been shown to lead to the dimer crystal structure, with the only problem that no continuous films could be obtained.[33] High-temperature mechanical rubbing proved to be a good alternative in this polymer (Figure 5). The existence of the dimer crystal structure is highlighted by the characteristic reflections at 10.5 and 5.8 Å in the ED pattern in Figure 5b.[33] Bright-field TEM images as well as AFM images of such films were recorded and can be seen in Figures 5c and 5d, respectively. In both the TEM and AFM images, lamellae perpendicular to the rubbing direction can be seen, consistent with polymer chain alignment. The semicrystalline nature of F-PCPDTBT is evidenced in the TEM image which shows alternating light and dark regions, corresponding to amorphous and crystalline domains within the polymer film. Polarized optical absorption spectroscopy was employed to assess the degree of alignment after HT rubbing. Through comparison of the ratio of intensities at the wavelength of maximum absorption, a moderate dichroic ratio of 2.3 was obtained (Figure S2a). Not surprisingly, it was also found that the absorption spectrum of the rubbed film is blue-shifted compared to the thin film spin-coated from chlorobenzene (see Figure 5e), and a new absorption maximum at 695 nm is observed. Accordingly for F-PCPDTBT, only two polymorphs were obtained: π-stacked and dimer. Again TEM did not give any evidence for coexistence of both polymorphs in our samples. We attribute the absence of the amorphous phase to the higher tendency of F-PCPDTBT to aggregate in solution as compared to C-PCPDTBT (see Figure 2).

2.4.2. Charge Transport Measurements. The hole mobilities of the different polymorphs of C- and F-PCPDTBT were evaluated using field-effect transistors in a top-gate bottom-

DOI: 10.1021/acs.macromol.6b01698
Macromolecules 2017, 50, 1402−1414

contact geometry (Table 3). This device architecture was employed since the same polymer interface investigated in

Table 3. Summary of Transistor Characteristics for All PCPDTBT Polymer Derivatives[a]

	morphology	μ_{sat} (cm^2/V s)
C-PCPDTBT (CB/DIO)	π-stacked (edge-on)[20]	$(8.6 \pm 1.0) \times 10^{-4}$
C-PCPDTBT (SVA-CS_2)	dimer	$(2.9 \pm 0.3) \times 10^{-4}$
C-PCPDTBT ($CHCl_3$)	amorphous	$(5.5 \pm 0.9) \times 10^{-4}$
F-PCPDTBT (CB)	π-stacked (edge-on)	$(2.5 \pm 0.2) \times 10^{-4}$
F-PCPDTBT (HT rubbed, ∥)	dimer	$(1.8 \pm 0.6) \times 10^{-4}$
F-PCPDTBT (HT rubbed, ⊥)	dimer	$(0.5 \pm 0.2) \times 10^{-4}$
Si-PCPDTBT (CB 80 °C)	cross-hatched	$(7.0 \pm 3.9) \times 10^{-3}$
Si-PCPDTBT (HT rubbed, ∥)	π-stacked (mostly face-on)	$(8.5 \pm 2.9) \times 10^{-3}$
Si-PCPDTBT (HT rubbed, ⊥)	π-stacked (mostly face-on)	$(0.6 \pm 0.1) \times 10^{-3}$
Si-PCPDTBT (HT rubbed, ∥) + ann 280 °C	π-stacked (mostly edge-on)	$(12.3 \pm 3.8) \times 10^{-3}$

[a]Mobility values were extracted from the transfer curves in the saturation regime and averaged over all channel lengths (50, 100, 150, and 200 μm) for 9−16 devices.

AFM is probed during transistor operation. The resulting output and transfer curves can be found in the Supporting Information (Figures S12 and S13). For C-PCPDTBT we found the following values: the π-stacked morphology (prepared from CB/DIO, Figure 4b) gave values of $(8.6 \pm 1.0) \times 10^{-4}$ $cm^2/(V\ s)$. This mobility is at the lower limit of mobility values reported in the literature (compare Table S1). Films containing the dimer crystal structure (prepared via solvent annealing, Figure 4c) gave average values of $(2.9 \pm 0.3) \times 10^{-4}$ $cm^2/(V\ s)$. The amorphous films (prepared from $CHCl_3$, Figure 4a) gave average values of $(5.5 \pm 0.9) \times 10^{-4}$ $cm^2/(V\ s)$. The dimer morphology and the amorphous film of C-PCPDTBT yield lower hole mobility values than the samples with long-range $\pi-\pi$ stacking. This result indicates that these structures are less suited for effective transport in FETs. In the case of the dimer structure this is likely due to the large distance between dimer units separated by the insulating alkyl chains. Although the dimer structure of the PCPDTBT chains is highly crystalline, transport can really only occur along the polymer chains.

In the case of F-PCPDTBT we compared π-stacked (prepared from CB, Figure 5a) vs dimer (prepared via HT-rubbing, Figure 5b−d) and found very similar charge carrier mobilities in the order of 2×10^{-4} $cm^2/(V\ s)$. In the literature charge carrier mobilities of F-PCPDTBT have been reported to be between 1×10^{-3} and 1.4×10^{-2} $cm^2/(V\ s)$ (compare Table S1),[21,22] which is 1−2 orders of magnitude higher than the values we measured. We attribute this difference to the low molecular weight of our polymer batch, as molecular weight has frequently been shown to be an important factor in determining charge carrier mobilities of conjugated polymers.[47,48]

The transistor characteristics of the HT rubbed film were obtained by rubbing in the direction parallel to the transport direction between source and drain contacts. We also performed the same rubbing experiments perpendicular to the transport direction, which gives a mobility of $(0.5 \pm 0.2) \times 10^{-4}$ $cm^2/(V\ s)$. The observation of anisotropic transport in these dimer structures indicates that charges are transported more efficiently along the conjugated backbones. Intermolecular transport occurs either via a superexchange mechanism, via tunneling over side chains, or through numerous structural defects, since these structures do not provide a direct electronic overlap between molecules. This charge transport anisotropy is in accordance with findings on P3HT and other D−A copolymers.[6,12,45]

Overall, one can conclude that the mobilities in these polymers remain quite low with $\pi-\pi$ stacking of the PCPDTBT chains best supporting charge transport in OFETs.

2.5. Si-PCPDTBT: Structural Analysis and Charge Transport. The last polymer in the series is the silicon-bridged cyclopentadithiophene analogue of PCPDTBT. It is also the least soluble material in the series, and due to its very high tendency to aggregate in solution, it was not possible to make homogeneous thin films using standard spin-coating conditions. We found that films of sufficient quality could be obtained by spin-coating from hot solutions of chlorobenzene (80 °C). The AFM phase image of the resulting film is displayed in Figure 6a and reveals round aggregates approximately 30 nm in diameter. Surprisingly, the HR-TEM image in Figure 6b evidences the formation of cross-hatched structures. Cross-hatched structures have been demonstrated for polypropylenes and poly(*p*-phenylene benzobisoxazole)[49] but were only recently reported for Si-PCPDTBT by Takacs and co-workers in very thin films.[50] The cross-hatched structures consist of alternating layers of polymer chains in which the angle between two chains from successive layers was found to be 53.6 ± 1.3°. This angle of 53.6° can be seen in the FFT pattern shown in the upper right-hand corner in Figure 6b, which reveals two clear sets of reflections 53.6° from one another. Incidentally, the same cross-hatched domains were also observed when aggregates of Si-PCPDTBT formed in solution were cast on a carbon-coated TEM grid, indicating that such aggregates are formed in solution and not upon drying during spin-coating (see Figure S11g,h). The periodicity between successive chains in a layer is around 17 Å, in agreement with earlier findings.[50] The absorption spectrum of the spin-coated thin film displays a maximum intensity at 765 nm (Figure 6d); this low-energy peak is attributed to arise from absorption from the aggregated species in the polymer film. We refer to the aggregation in chlorobenzene solution in Figure 2c.

High-temperature rubbing experiments were conducted at 230 °C in order to align the chains and to explore if the dimer structure can be obtained for Si-PCPDTBT. A representative HR-TEM image is shown in Figure 6e. As seen in Figure 6f, the ED pattern of the rubbed films shows a strong 0 0 4 reflection at 5.7 Å along the rubbing direction, indicating high alignment of the chains (consistent with the chain periodicity along the backbone direction). Along the equator, the ED pattern shows a strong reflection at 17.1 Å. Moreover, HR TEM shows clearly a fringed pattern with a period of 17.4 Å. Despite the same interchain period of around 17 Å, the rubbed films did not give any evidence for cross-hatched structures as observed in the spin-coated films. The contrast in this pattern arises from the density contrast between layers of π-stacked Si-PCPDTBT backbones and layers of alkyl side chains. Si-PCPDTBT chains are well π-stacked and form aligned crystals in face-on orientation in the rubbed films. Interestingly, the Si-PCPDTBT films do not show a periodic semicrystalline morphology as was found for the rubbed F-PCPDTBT samples (compare Figures 5c and 5d). For comparison, Si-PCPDTBT spin-coated and

DOI: 10.1021/acs.macromol.6b01698
Macromolecules 2017, 50, 1402−1414

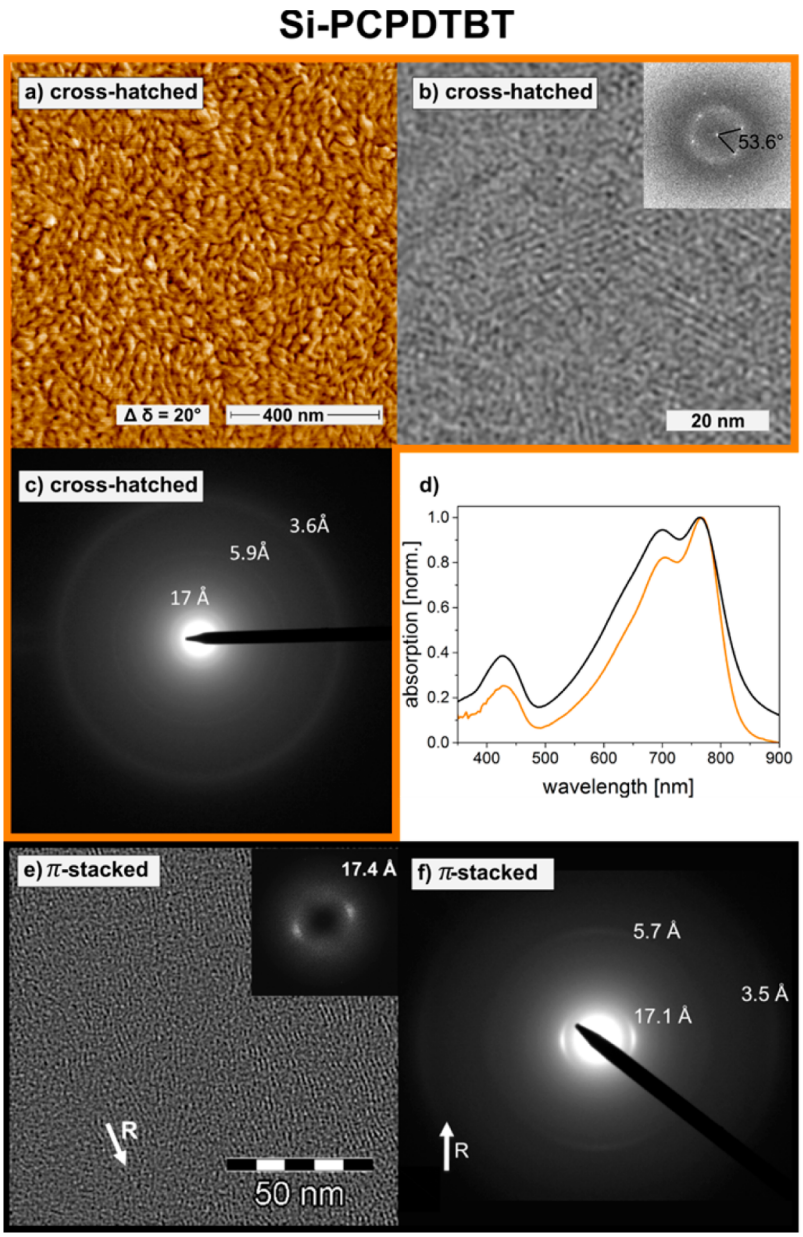

Figure 6. (a) AFM phase image of Si-PCPDTBT spin-coated from CB at 80 °C. (b) HR-TEM image and (c) corresponding ED pattern of spin-coated sample. (d) Absorption profile of spin-coated (orange) and rubbed film (black), respectively. (e) HR-TEM image after HT rubbing at 230 °C. (f) ED pattern of Si-PCPDTBT after HT rubbing at 230 °C. For further morphological data on Si-PCPDTBT we refer to Figures S10 and S11.

drop-cast films also consist rather of flake-like or whisker-like domains (see AFM image Figure 6a and bright-field TEM image in Figure S11d,g).

The absorption profile of the thin film after rubbing is plotted in Figure 6d and has a λ_{max} around 760 nm as well as a shoulder around 700 nm. Overall, the absorption profile of the dominantly face-on, π-stacked arrangement is similar to the films containing cross-hatched morphologies. Linear polarized optical absorption spectroscopy of the rubbed films (plotted in Figure S2b) yielded a moderate dichroic ratio of 2.1, indicating that polymer chain alignment was to some extent successful after rubbing. As a point of reference, using the same rubbing technique on P3HT films, dichroic ratios up to 25 have been observed.[45]

The rubbed films were further exposed to postannealing treatment close to the polymer melting point. ED suggests that thermal annealing of the rubbed films at T = 280 °C results in a change of the crystal orientation from dominant face-on to dominant edge-on with an increased intensity of the characteristic 3.5 Å π-stacking peak, a sharper 5.7 Å reflection, and the fading of the 100 reflection at 17.4 Å (Figure S10i). Therefore, ED does not evidence a change in the polymorphism of Si-PCPDTBT upon thermal annealing but only a reorientation of the crystals. In other words, the π-stacked structure in Si-PCPDTBT is thermodynamically stable up to high temperatures close to the polymer melting and does not transform to a dimer-like structure.

For the silicon-containing analogue, the hole mobility of the predominately cross-hatched oriented morphology (spin-coated sample) is compared to that of the mostly face-on oriented π-stacked chains (HT-rubbing) (Table 3). In both cases, all transistor characteristics were very similar, and

DOI: 10.1021/acs.macromol.6b01698
Macromolecules 2017, 50, 1402−1414

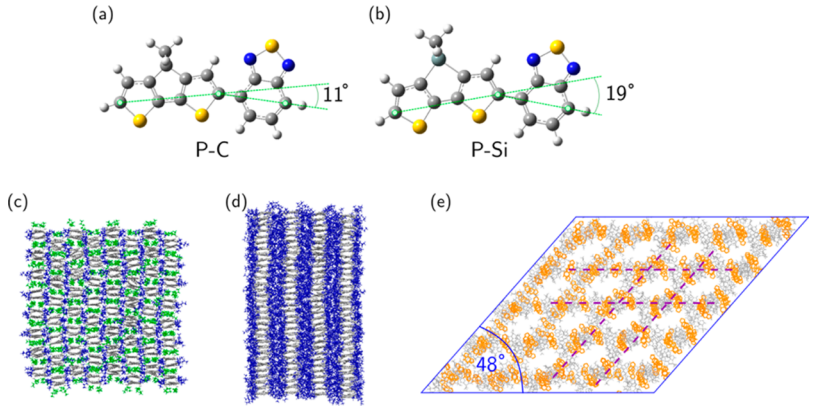

Figure 7. Optimized geometries of one repeat unit for C-PCPDTBT (a) and Si-PCPDTBT (b) highlighting the effect of substituting the bridged carbon atom in the cyclopentadithiophene with silicon. Supercells of the three different packing motifs: dimer (c), π-stacked (d), and cross-hatched (e). The cross-hatched morphology was obtained by equilibrating (molecular dynamics, 300 K, NPT ensemble) a supercell[50] of decamers.

mobility values around 10^{-2} $cm^2/(V\ s)$ were obtained which is comparable to reported mobilities (compare Table S1). Although additional thermal annealing at 280 °C of the mechanically rubbed film led to a clear enhancement of the intensity of the ED reflections, no significant effect could be seen on the hole mobilities. Overall, these findings indicate that there is little effect of the two different packing motifs on the charge transport in FETs for Si-PCPDTBT.

2.6. Discussion. This study has shown that depending on the processing conditions, one can access three different polymorphs in the PCPDTBT family. Figures 7c,d,e show supercells of the three packing motifs for illustration: dimer-like (c), π-stacked (d), and cross-hatched (e) structures.

In the case of C-PCPDTBT it is possible to access both an amorphous and π-stacked film morphology by varying the deposition solvent, whereas for the other two polymers, F-PCPDTBT and Si-PCPDTBT, we could not find the appropriate conditions to make amorphous films. We believe this is due to increased tendency for the polymers to aggregate within the series C-PCPDTBT, F-PCPDTBT, and Si-PCPDTBT. In fact, the backbone stiffness, evaluated from the scans of the dihedral potentials between the donor and acceptor units of the backbone (Figure S3), was found to be similar for all three polymers, indicating that solvent−polymer interactions play a dominant role in determining polymer film properties.

For all three polymers we could access π-stacked morphologies. In the case of C-PCPDTBT the addition of diiodooctane to the processing solvent was required, while F-PCPDTBT formed π -stacked structures upon deposition from CB. Both polymers form edge-on textures on substrates. For Si-PCPDTBT we found π-stacked structures upon high temperature rubbing. While mostly face-on textures were observed directly after HT rubbing, additional annealing at 280 °C led to mostly edge-on domains. The π-stacking distance follows the sequence 3.75 Å (C-PCPDTBT), 3.7 Å (F-PCPDTBT), and 3.5 Å (Si-PCPDTBT). The interlayer spacings are around 17 Å for Si-PCPDTBT and around 11 Å for C- and F-PCPDTBT.

The dimer-like packing motif was exclusively found for F- and C-PCPDTBT. It can be accessed by applying techniques at temperatures close to the melting of the polymer such as high-temperature mechanical rubbing and melt crystallization on friction-transferred PTFE substrates or solvent vapor annealing.[33] The data suggest that this crystal structure is the thermodynamically stable polymorph for these two polymers.

The silicon-containing polymer shows no evidence of dimer-like packing. Even temperature annealing after high temperature rubbing did not lead to the dimer structures. On the other hand, cross-hatched structures are observed exclusively for Si-PCPDTBT. The finding that both the cross-hatched and the π-stacked motifs reveal an interlayer spacing of 17 Å raises the question on the origin of the cross-hatched structure, that means if it is a new crystal structure or do defects in the π-stacked structure, e.g., by twinning, induce the formation of it?

From the standpoint of charge transport, OFET measurements show that the highest charge mobilities are observed for Si-PCPDTBT films. This is consistent with reports from literature (compare Table S1). Simulations of charge mobilities showed that local ordering tends to favor transport in Si-PCPDTBT as compared to the other derivatives. However, the difference in simulated mobilities is smaller than that measured in OFETs, suggesting that large-scale structural and morphological aspects play a role as well. In particular, the difference in polymorphism between the analogues should have some impact on charge transport.

Our findings open the question on the origin of the polymorphism in this homologous series of polymers and how this polymorphism affects charge transport. From a molecular point of view, Si-PCPDTBT is different from the other two polymers regarding the backbone conformation. Indeed, as seen in Figures 7a,b, the backbone conformations of both classes of polymers are clearly distinct regarding the angle ϕ between the cyclopentadithiophene and the benzodithiazole units. It is equal to 11° for C-PCPDTBT and F-PCPDTBT versus 19° for Si-PCPDTBT. Such a difference in ϕ can impact the packing of the chains and in particular the π -stacking since the bulky diethylhexyl side chains have to be accommodated on either side of the layers of that π-stacked backbones. The higher value of ϕ for Si-PCPDTBT should translate to a larger layer period as compared to the other analogues. This is indeed observed experimentally: only for Si-PCPDTBT a large interlayer period of 17 Å is observed versus 11 Å for the other analogues. Moreover, the large ϕ enables a new packing of chains into layers in which the directions of the chains make a regular angle in Si-PCPDTBT and generates the cross-hatched patterns observed by TEM. Apparently no such cross-hatched chain packing is possible for C-PCPDTBT or F-

DOI: 10.1021/acs.macromol.6b01698
Macromolecules 2017, 50, 1402−1414

PCPDTBT because of the smaller value of ϕ. Takacs and co-workers suggested that the cross-hatched patterns are due to layers of chains with two in-plane directions making a relative angle of 53° as shown in Figures 6b and 7e.[50] It has been proposed that such cross-hatched domains help to interconnect nanocrystals with different in-plane orientations and thus help to create quasi-three-dimensional transport pathways (two directions in-plane plus π-stacking perpendicular to the substrate plane). The situation is different for both the classical π-stacked and the dimer polymorphs observed for C-PCPDTBT and F-PCPDTBT. For these systems, charge transport should be essentially 2D in the π-stacked crystals and even 1D in the dimer structure. Macroscopic charge transport in C-PCPDTBT and F-PCPDTBT will imply charges to transit between ordered domains but without the highly interconnected domains found for Si-PCPDTBT. Accordingly, the comparison of charge transport in the analogous series of PCPDTBTs highlights the essential role of polymorphism that is at least in part controlled by a molecular parameter, i.e., the ϕ angle in the conjugated backbone conformation.

In other words, this is one of the first examples that illustrates how a change in the backbone conformation of a homologous series of polymers results in different packing motives of the chains in a crystal. Moreover, these correlations between backbone structure and packing coincide with differences in hole mobilities.

3. CONCLUSION

PCPDTBT-based low band gap polymers showed the formation of aggregates both in solution and when deposited as thin films. Amorphous, π-stacked, cross-hatched, or dimer polymorphs can be obtained by adjusting the processing conditions (solvent, temperature, rubbing, etc.). Both experimentally measured and computer simulated hole mobilities confirmed that the $\pi-\pi$ stacked Si-PCPDTBT derivative has the highest mobilities in the series, which is also in agreement with literature (Table S1). Simulations showed that going from the carbon to the fluorine to the silicon derivative, the local charge mobility of the $\pi-\pi$ stacked systems increased. This increase is due to a better registry of the polymer chain backbones and more optimized packing of side chains, which leads to larger effective electronic coupling elements. The dimer-based and the amorphous thin films demonstrated lower mobility values than the π-stacked and cross-hatched structures. For the dimer-containing morphology, it seems likely that the transport is limited to one direction (along the polymer chain) as the bulky alkyl side chains create a large gap between dimer units. On the whole, small changes in the polymer structure drastically modified aggregation and solubility behavior, thereby strongly influencing the extent of morphology tunability. C-PCPDTBT was the most versatile in the series, next came F-PCPDTBT, and finally Si-PCPDTBT. The observed differences in chain packing, i.e., dimer-like versus cross-hatched, are attributable, at least in part, to the differences in backbone conformations.

4. EXPERIMENTAL SECTION

Materials. Poly[2,6-(4,4-bis(2-ethylhexyl)-4*H*-cyclopenta[2,1-*b*;3,4-*b*′]dithiophene)-*alt*-4,7-(2,1,3-benzothiadiazole)] (PCPDTBT) was purchased from 1-Material. Poly[2,6-(4,4-bis(2-ethylhexyl)-4*H*-cyclopenta[2,1-*b*;3,4-*b*′]dithiophene)-*alt*-4,7-(5-fluoro-2,1,3-benzothiadiazole)] (F-PCPDTBT) was synthesized by the group of S. Janietz at the Fraunhofer Institut für Angewandte Polymerforschung in Potsdam. Poly[(4,4′-bis(2-ethylhexyl)dithiene-[3,2-*b*:2′,3′-*d*]silole)-*alt*-4,7-(2,1,3-benzothiadiazole)] (Si-PCPDTBT) was bought from Konarka. All solvents (chlorobenzene, THF, $CHCl_3$, 1,8-diiodooctane, butyl acetate) were purchased from Sigma-Aldrich (p.a. grade). Molecular weights were determined by high-temperature gel permeation chromatography in trichlorobenzene at 160 °C versus polystyrene standards. Absorption solution spectra were measured with a Zeiss spectrometer (light source: CLH600, detector: MCS621 VIS II and MCS611 NIR 2.2 μm) in transmission mode using fiber optics.

Film Processing. As substrates 1 × 1 cm^2 microscope slides (for UV−vis absorption), pure Si wafers (for AFM), and Si wafers with a 300 nm SiOx layer (for TEM) were employed and cleaned with a CO_2 snow jet followed by exposure to oxygen plasma (Diener Femto 100 W) for at least 600 s. Both solution and film preparations were done under a nitrogen atmosphere. The solvent-additive processed films were prepared from 3 mg/mL CB solutions in the presence of 2 wt % DIO; spin-coating was performed at 1500 rpm for 300 s. The initial films for solvent vapor annealing were prepared from 3 mg/mL $CHCl_3$ solutions. The films were prepared by spin-coating at 1500 rpm for 30 s within 24 h after preparation of the solutions. For solvent vapor annealing $CHCl_3$ precast films were exposed to controlled CS_2 vapor as previously described.[32] The films were swollen to a solution like state at a vapor pressure of 92%; recrystallization was induced by decreasing the vapor pressure first to 88% and then to 85% within 10 min. The temperature of the vapor was set to 22 °C and the sample temperature to 20 °C. The F-PCPDTBT thin films were deposited from CB solution (3 mg/mL), and the Si-PCPDTBT films were also made from 3 mg/mL solutions deposited at 80 °C. High-temperature rubbing of the F-PCPDTBT thin films was performed following a procedure described in the literature.[33] The rubbing was performed at 240 °C by applying a rotating cylinder equipped with a fiber cloth with a pressure of 2 bar on the sample holder. High-temperature rubbing of the Si-PCPDTBT films was performed at 230 °C.

Film Characterization. Oriented areas were identified for transmission electron microscopy (TEM) analysis by optical microscopy (Leica DMR-X microscope). The polymer films were coated with a thin amorphous carbon film and removed from the glass substrates by floating on a diluted aqueous HF solution (5 wt %) and subsequently recovered on TEM copper grids. Aggregates present in solution were studied by drop-casting CB solutions on TEM copper grids. TEM was performed in bright-field, high-resolution, and diffraction modes using a CM12 Philips microscope equipped with a MVIII (Soft Imaging System) charge coupled device camera. Calibration of the reticular distances in the ED patterns was made with an oriented PTFE film. UV−vis−NIR spectroscopy was performed with a Zeiss spectrometer (light source: CLH600, detector: MCS621 VIS II and MCS611 NIR 2.2 μm) in transmission mode using fiber optics. AFM was performed on a Dimension Icon AFM from Bruker operating in tapping mode.

Organic Field-Effect Transistors. Charge transport was probed in organic field-effect transistors in a top-gate bottom-contact geometry in a nitrogen atmosphere. Gold source and drain electrodes of 30 nm thickness with a 5 nm thick chromium adhesion layer were evaporated using a shadow mask on glass substrates defining transistor channels with a channel length (L) of 100−250 μm and channel width (W) of 1 mm. The transistor substrates were cleaned by successive ultrasonication in acetone and isopropanol each for 10 min, rinsing in isopropanol, and drying in a nitrogen stream. The polymer solution was prepared in the glovebox by stirring at elevated temperature for at least 4 h to allow complete dissolution of the polymer. Poly(methyl methacrylate) (PMMA) layers (500 nm) (EG-PMMA, M_n = 300 kDa, purchased from Polymer Source Inc.) served as dielectric and were spin-coated from *n*-butyl acetate (60 mg/mL) followed by annealing at 80 °C for 30 min. In a last step, aluminum (30 nm) was evaporated through a shadow mask and used as gate electrode. Transistor testing was performed with a SUSS Microtech setup connected to a Keithley 2636 Source meter under inert atmosphere. The charge carrier mobilities were extracted from the saturation regime at −60 V using $I_{SD} = \frac{W}{2L}\mu C_i(V_G - V_T)^2$, where I_{SD} the source-drain current, C_i is the

DOI: 10.1021/acs.macromol.6b01698
Macromolecules 2017, 50, 1402−1414

capacitance per unit area, and V_G is the gate voltage. Mobilities were averaged over all channels lengths (50, 100, 150, and 200 μm) for 9–16 devices.

Simulation Methods. In this paper, MD simulations of C-/F- and Si-PCPDTBT morphologies were performed using the GROMACS simulation package[51] (v 4.6.7). Charge transfer integrals, site energies, and mobilities were evaluated using a combination of the Gaussian G09 simulation package[52] and the VOTCA-CTP module.[40]

■ ASSOCIATED CONTENT

Supporting Information

The Supporting Information is available free of charge on the ACS Publications website at DOI: 10.1021/acs.macromol.6b01698.

Figures S1–S14 and Table S1 (PDF)

■ AUTHOR INFORMATION

Corresponding Author

*E-mail sabine.ludwigs@ipoc.uni-stuttgart.de (S.L.).

ORCID

S. Ludwigs: 0000-0002-6717-8538

Notes

The authors declare no competing financial interest.

■ ACKNOWLEDGMENTS

This work was supported in part by the Deutsche Forschungsgemeinschaft (DFG) under the Emmy Noether program, the Priority Program "Elementary Processes of Organic Photovoltaics" (SPP 1355), IRTG 1404 and TRR146, and the BMBF grants MESOMERIE (FKZ 13N10723) and MEDOS (FKZ 03EK3503B). The project has further received funding from the NMP-20-2014–"Widening materials models" program under grant agreement no. 646259 (MOSTOPHOS) and the Stuttgart-Strasbourg project through PROCOPE (DAAD). We are very grateful to S. Janietz, who provided us with F-PCPDTBT, and H. Klauk, U. Zschieschang, R. di Pietro, and S. Tannert for support with the transistor measurements.

■ REFERENCES

(1) Tremel, K.; Ludwigs, S. Morphology of P3HT in Thin Films in Relation to Optical and Electrical Properties. In *P3HT Revisited - From Molecular Scale to Solar Cell Devices*; Ludwigs, S., Ed.; Springer: Berlin, 2014; Vol. *265*, pp 39–82.

(2) Sirringhaus, H.; Brown, P. J.; Friend, R. H.; Nielsen, M. M.; Bechgaard, K.; Langeveld-Voss, B. M. W.; Spiering, A. J. H.; Janssen, R. A. J.; Meijer, E. W.; Herwig, P.; et al. Two-Dimensional Charge Transport in Self-Organized, High-Mobility Conjugated Polymers. *Nature* **1999**, *401*, 685–688.

(3) Poelking, C.; Daoulas, K.; Troisi, A.; Andrienko, D. Morphology and Charge Transport in P3HT: A Theorist's Perspective. In *P3HT Revisited – From Molecular Scale to Solar Cell Devices*; Ludwigs, S., Ed.; Springer: Berlin, 2014; Vol. *265*, pp 139–180.

(4) Poelking, C.; Andrienko, D. Effect of Polymorphism, Regioregularity and Paracrystallinity on Charge Transport in Poly(3-Hexylthiophene) [P3HT] Nanofibers. *Macromolecules* **2013**, *46*, 8941–8956.

(5) Crossland, E. J. W.; Rahimi, K.; Reiter, G.; Steiner, U.; Ludwigs, S. Systematic Control of Nucleation Density in Poly(3-Hexylthiophene) Thin Films. *Adv. Funct. Mater.* **2011**, *21* (3), 518–524.

(6) Crossland, E. J. W.; Tremel, K.; Fischer, F. S. U.; Rahimi, K.; Reiter, G.; Steiner, U.; Ludwigs, S. Anisotropic Charge Transport in Spherulitic Poly(3-Hexylthiophene) Films. *Adv. Mater.* **2012**, *24*, 839–844.

(7) Leclerc, M. Polyfluorenes: Twenty Years of Progress. *J. Polym. Sci., Part A: Polym. Chem.* **2001**, *39*, 2867–2873.

(8) Grell, M.; Bradley, D. D. C.; Ungar, G.; Hill, J.; Whitehead, K. S. Interplay of Physical Structure and Photophysics for a Liquid Crystalline Polyfluorene. *Macromolecules* **1999**, *32*, 5810–5817.

(9) Brinkmann, M. Directional Epitaxial Crystallization and Tentative Crystal Structure of Poly(9,9′-Di-N-Octyl-2,7-Fluorene). *Macromolecules* **2007**, *40* (21), 7532–7541.

(10) Yan, H.; Chen, Z.; Zheng, Y.; Newman, C.; Quinn, J. R.; Dötz, F.; Kastler, M.; Facchetti, A. A High-Mobility Electron-Transporting Polymer for Printed Transistors. *Nature* **2009**, *457*, 679–686.

(11) Kang, H.; Uddin, M. A.; Lee, C.; Kim, K. H.; Nguyen, T. L.; Lee, W.; Li, Y.; Wang, C.; Woo, H. Y.; Kim, B. J. Determining the Role of Polymer Molecular Weight for High-Performance All-Polymer Solar Cells: Its Effect on Polymer Aggregation and Phase Separation. *J. Am. Chem. Soc.* **2015**, *137*, 2359–2365.

(12) Tremel, K.; Fischer, F. S. U.; Kayunkid, N.; Di Pietro, R.; Tkachov, R.; Kiriy, A.; Neher, D.; Ludwigs, S.; Brinkmann, M. Charge Transport Anisotropy in Highly Oriented Thin Films of the Acceptor Polymer P(NDI2OD-T2). *Adv. Energy Mater.* **2014**, *4*, 1301659.

(13) Brinkmann, M.; Gonthier, E.; Bogen, S.; Tremel, K.; Ludwigs, S.; Hufnagel, M.; Sommer, M. Segregated versus Mixed Interchain Stacking in Highly Oriented Films of Naphthalene Diimide Bithiophene Copolymers. *ACS Nano* **2012**, *6*, 10319–10326.

(14) Mühlbacher, D.; Scharber, M.; Morana, M.; Zhu, Z.; Waller, D.; Gaudiana, R.; Brabec, C. High Photovoltaic Performance of a Low-Bandgap Polymer. *Adv. Mater.* **2006**, *18*, 2884–2889.

(15) Peet, J.; Kim, J. Y.; Coates, N. E.; Ma, W. L.; Moses, D.; Heeger, A. J.; Bazan, G. C. Efficiency Enhancement in Low-Bandgap Polymer Solar Cells by Processing with Alkane Dithiols. *Nat. Mater.* **2007**, *6*, 497–500.

(16) Peet, J.; Cho, N. S.; Lee, S. K.; Bazan, G. C. Transition from Solution to the Solid State in Polymer Solar Cells Cast from Mixed Solvents. *Macromolecules* **2008**, *41*, 8655–8659.

(17) Agostinelli, T.; Ferenczi, T. a. M.; Pires, E.; Foster, S.; Maurano, A.; Müller, C.; Ballantyne, A.; Hampton, M.; Lilliu, S.; Campoy-Quiles, M.; et al. The Role of Alkane Dithiols in Controlling Polymer Crystallization in Small Band Gap polymer:Fullerene Solar Cells. *J. Polym. Sci., Part B: Polym. Phys.* **2011**, *49*, 717–724.

(18) Rogers, J. T.; Schmidt, K.; Toney, M. F.; Kramer, E. J.; Bazan, G. C. Structural Order in Bulk Heterojunction Films Prepared with Solvent Additives. *Adv. Mater.* **2011**, *23*, 2284–2288.

(19) Rogers, J. T.; Schmidt, K.; Toney, M. F.; Bazan, G. C.; Kramer, E. J. Time-Resolved Structural Evolution of Additive-Processed Bulk Heterojunction Solar Cells. *J. Am. Chem. Soc.* **2012**, *134*, 2884–2887.

(20) Gu, Y.; Wang, C.; Russell, T. P. Multi-Length-Scale Morphologies in PCPDTBT/PCBM Bulk-Heterojunction Solar Cells. *Adv. Energy Mater.* **2012**, *2*, 683–690.

(21) Albrecht, S.; Janietz, S.; Schindler, W.; Frisch, J.; Kurpiers, J.; Kniepert, J.; Inal, S.; Pingel, P.; Fostiropoulos, K.; Koch, N.; et al. Fluorinated Copolymer PCPDTBT with Enhanced Open-Circuit Voltage and Reduced Recombination for Highly Efficient Polymer Solar Cells. *J. Am. Chem. Soc.* **2012**, *134*, 14932–14944.

(22) Zhang, Y.; Zou, J.; Cheuh, C.; Yip, H.; Jen, A. K.-Y. Significant Improved Performance of Photovoltaic Cells Made from a Partially Fluorinated Cyclopentadithiophene/Benzothiadiazole Conjugated Polymer. *Macromolecules* **2012**, *45*, 5427–5435.

(23) Chang, C. Y.; Zuo, L.; Yip, H. L.; Li, Y.; Li, C. Z.; Hsu, C. S.; Cheng, Y. J.; Chen, H.; Jen, A. K. Y. A Versatile Fluoro-Containing Low-Bandgap Polymer for Efficient Semitransparent and Tandem Polymer Solar Cells. *Adv. Funct. Mater.* **2013**, *23*, 5084–5090.

(24) Li, Y.; Zou, J.; Yip, H.-L.; Li, C.-Z.; Zhang, Y.; Chueh, C.-C.; Intemann, J.; Xu, Y.; Liang, P.-W.; Chen, Y.; et al. Side-Chain Effect on Cyclopentadithiophene/Fluorobenzothiadiazole-Based Low Band Gap Polymers and Their Applications for Polymer Solar Cells. *Macromolecules* **2013**, *46*, 5497–5503.

(25) Hou, J.; Chen, H.-Y.; Zhang, S.; Li, G.; Yang, Y. Synthesis, Characterization, and Photovoltaic Properties of a Low Band Gap

DOI: 10.1021/acs.macromol.6b01698
Macromolecules 2017, 50, 1402–1414

Polymer Based on Silole-Containing Polythiophenes and 2,1,3-Benzothiadiazole. *J. Am. Chem. Soc.* **2008**, *130*, 16144−16145.
(26) Morana, M.; Azimi, H.; Dennler, G.; Egelhaaf, H. J.; Scharber, M.; Forberich, K.; Hauch, J.; Gaudiana, R.; Waller, D.; Zhu, Z. H.; et al. Nanomorphology and Charge Generation in Bulk Heterojunctions Based on Low-Bandgap Dithiophene Polymers with Different Bridging Atoms. *Adv. Funct. Mater.* **2010**, *20*, 1180−1188.
(27) Albrecht, S.; Vandewal, K.; Tumbleston, J. R.; Fischer, F. S. U.; Douglas, J. D.; Fréchet, J. M. J.; Ludwigs, S.; Ade, H.; Salleo, A.; Neher, D. On the Efficiency of Charge Transfer State Splitting in Polymer:Fullerene Solar Cells. *Adv. Mater.* **2014**, *26*, 2533−2539.
(28) Chen, H.-Y.; Hou, J.; Hayden, A. E.; Yang, H.; Houk, K. N.; Yang, Y. Silicon Atom Substitution Enhances Interchain Packing in a Thiophene-Based Polymer System. *Adv. Mater.* **2010**, *22*, 371−375.
(29) Scharber, M. C.; Koppe, M.; Gao, J.; Cordella, F.; Loi, M. A.; Denk, P.; Morana, M.; Egelhaaf, H.-J.; Forberich, K.; Dennler, G.; et al. Influence of the Bridging Atom on the Performance of a Low-Bandgap Bulk Heterojunction Solar Cell. *Adv. Mater.* **2010**, *22*, 367−370.
(30) Scharsich, C.; Fischer, F. S. U.; Wilma, K.; Hildner, R.; Ludwigs, S.; Köhler, A. Revealing Structure Formation in PCPDTBT by Optical Spectroscopy. *J. Polym. Sci., Part B: Polym. Phys.* **2015**, *53*, 1416−1430.
(31) Fischer, F. S. U.; Tremel, K.; Saur, A.-K.; Link, S.; Kayunkid, N.; Brinkmann, M.; Herrero-Carvajal, D.; Navarrete, J. T. L.; Delgado, M. C. R.; Ludwigs, S. Influence of Processing Solvents on Optical Properties and Morphology of a Semicrystalline Low Bandgap Polymer in the Neutral and Charged States. *Macromolecules* **2013**, *46*, 4924−4931.
(32) Fischer, F. S. U.; Trefz, D.; Back, J.; Kayunkid, N.; Tornow, B.; Albrecht, S.; Yager, K. G.; Singh, G.; Karim, A.; Neher, D.; et al. Highly Crystalline Films of PCPDTBT with Branched Side Chains by Solvent Vapor Crystallization: Influence on Opto-Electronic Properties. *Adv. Mater.* **2015**, *27*, 1223−1228.
(33) Fischer, F. S. U.; Kayunkid, N.; Trefz, D.; Ludwigs, S.; Brinkmann, M. Structural Models of Poly(cyclopentadithiophene- Alt -Benzothiadiazole) with Branched Side Chains: Impact of a Single Fluorine Atom on the Crystal Structure and Polymorphism of a Conjugated Polymer. *Macromolecules* **2015**, *48*, 3974−3982.
(34) Horie, M.; Kettle, J.; Yu, C.-Y.; Majewski, L. A.; Chang, S.-W.; Kirkpatrick, J.; Tuladhar, S. M.; Nelson, J.; Saunders, B. R.; Turner, M. L. Cyclopentadithiophene-Benzothiadiazole Oligomers and Polymers; Synthesis, Characterisation, Field-Effect Transistor and Photovoltaic Characteristics. *J. Mater. Chem.* **2012**, *22*, 381−389.
(35) Kettle, J.; Horie, M.; Majewski, L. A.; Saunders, B. R.; Tuladhar, S.; Nelson, J.; Turner, M. L. Optimisation of PCPDTBT Solar Cells Using Polymer Synthesis with Suzuki Coupling. *Sol. Energy Mater. Sol. Cells* **2011**, *95*, 2186−2193.
(36) Baumeier, B.; Kirkpatrick, J.; Andrienko, D. Density-Functional Based Determination of Intermolecular Charge Transfer Properties for Large-Scale Morphologies. *Phys. Chem. Chem. Phys.* **2010**, *12*, 11103−11113.
(37) Becke, A. D. Density-Functional Thermochemistry. III. The Role of Exact Exchange. *J. Chem. Phys.* **1993**, *98*, 5648.
(38) Berendsen, H. J. C.; Postma, J. P. M.; van Gunsteren, W. F.; DiNola, A.; Haak, J. R. Molecular Dynamics with Coupling to an External Bath. *J. Chem. Phys.* **1984**, *81*, 3684.
(39) Marcus, R. A. On the Theory of Oxidation-Reduction Reactions Involving Electron Transfer. I. *J. Chem. Phys.* **1956**, *24*, 966.
(40) Rühle, V.; Lukyanov, A.; May, F.; Schrader, M.; Vehoff, T.; Kirkpatrick, J.; Baumeier, B.; Andrienko, D. Microscopic Simulations of Charge Transport in Disordered Organic Semiconductors. *J. Chem. Theory Comput.* **2011**, *7*, 3335−3345.
(41) Poelking, C.; Andrienko, D. Long-Range Embedding of Molecular Ions and Excitations in a Polarizable Molecular Environment. *J. Chem. Theory Comput.* **2016**, *12*, 4516−4523.
(42) Jansen, A. P. J. An Introduction to Monte Carlo Simulations of Surface Reactions. *arXiv*, 2003.
(43) Guilbert, A. A. Y.; Frost, J. M.; Agostinelli, T.; Pires, E.; Lilliu, S.; Macdonald, J. E.; Nelson, J. Influence of Bridging Atom and Side Chains on the Structure and Crystallinity of Cyclopentadithiophene−Benzothiadiazole Polymers. *Chem. Mater.* **2014**, *26*, 1226−1233.
(44) Yamashita, Y.; Hinkel, F.; Marszalek, T.; Zajaczkowski, W.; Pisula, W.; Baumgarten, M.; Matsui, H.; Müllen, K.; Takeya, J. Mobility Exceeding 10 cm2 /Vs in Donor-Acceptor Polymer Transistors with Band-like Charge Transport. *Chem. Mater.* **2016**, *28*, 420−424.
(45) Hamidi-Sakr, A.; Biniek, L.; Fall, S.; Brinkmann, M. Precise Control of Lamellar Thickness in Highly Oriented Regioregular Poly(3-Hexylthiophene) Thin Films Prepared by High-Temperature Rubbing: Correlations with Optical Properties and Charge Transport. *Adv. Funct. Mater.* **2016**, *26*, 408−420.
(46) Fischer, F. S. U. *The Impact of Donor-Acceptor Polymer Crystal Structure and Mesoscopic Morphology on Opto-Electronic Devices*; University of Stuttgart: 2015.
(47) Tsao, H. N.; Cho, D. M.; Park, I.; Hansen, M. R.; Mavrinskiy, A.; Yoon, D. Y.; Graf, R.; Pisula, W.; Spiess, H. W.; Müllen, K. Ultrahigh Mobility in Polymer Field-Effect Transistors by Design. *J. Am. Chem. Soc.* **2011**, *133*, 2605−2612.
(48) Morana, M.; Wegscheider, M.; Bonanni, A.; Kopidakis, N.; Shaheen, S.; Scharber, M.; Zhu, Z.; Waller, D.; Gaudiana, R.; Brabec, C. J. Bipolar Charge Transport in PCPDTBT-PCBM Bulk-Heterojunctions for Photovoltaic Applications. *Adv. Funct. Mater.* **2008**, *18*, 1757−1766.
(49) Martin, D. C.; Thomas, E. L. Grain Boundaries in Extended-Chain Polymers: Theory and Experiment. *Philos. Mag. A* **1991**, *64*, 903−922.
(50) Takacs, C. J.; Brady, M. A.; Treat, N. D.; Kramer, E. J.; Chabinyc, M. L. Quadrites and Crossed-Chain Crystal Structures in Polymer Semiconductors. *Nano Lett.* **2014**, *14*, 3096−3101.
(51) Pall, S.; Abraham, M. J.; Kutzner, C.; Hess, B.; Lindahl, E. Tackling Exascale Software Challenges in Molecular Dynamics Simulations with GROMACS. In *Solving Software Challenges for Exascale*; Markidis, S., Laure, E., Eds.; Springer: Berlin, 2014; pp 3−27.
(52) Frisch, M. J.; Trucks, G. W.; Schlegel, H. B.; Scuseria, G. E.; Robb, M. A.; Cheeseman, J. R.; Scalmani, G.; Barone, V.; Mennucci, B.; Petersson, G. A.; et al. *Gaussian 09*; 2009.

DOI: 10.1021/acs.macromol.6b01698
Macromolecules 2017, 50, 1402−1414